Supplementary Information

High-field liquid state NMR hyperpolarization:

A combined DNP/NMRD approach

Petr Neugebauer[a], Jan G. Krummenacker[a], Vasyl P. Denysenkov[a], Christina Helmling[a], Claudio Luchinat[b], Giacomo Parigi[b]* and Thomas F. Prisner[a]*

[a] *Institute of Physical and Theoretical Chemistry and Center for Biomolecular Magnetic Resonance (BMRZ), Goethe-University, Max-von-Laue-Str. 7, 60438, Frankfurt am Main, Germany.*

[b] *Magnetic Resonance Center (CERM) and Department of Chemistry, University of Florence, Via L. Sacconi 6, Florence, Italy*

1) Heisenberg spin exchange rates determined from X-band and G-band cw-EPR spectra
2) Rotational correlation times determined from X-band and G-band cw-EPR spectra
3) Temperature calibration of samples under DNP conditions
4) Leakage factor determination at different temperatures and radical concentrations
5) Saturation parameter as a function of MW power
6) NMRD experiments

1) Heisenberg spin exchange rates determined from X-band and G-band cw-EPR spectra

The EPR linewidth was measured at G-band frequencies (180 GHz / 6.4 T) as a function of the TEMPOL radical concentration for all solvents. Narrowing of the hyperfine split EPR signal by Heisenberg spin exchange could be observed for all solvents for higher concentrations (> 10-100 mM). At very high concentrations broadening of the single EPR line by dipolar relaxation could be observed.

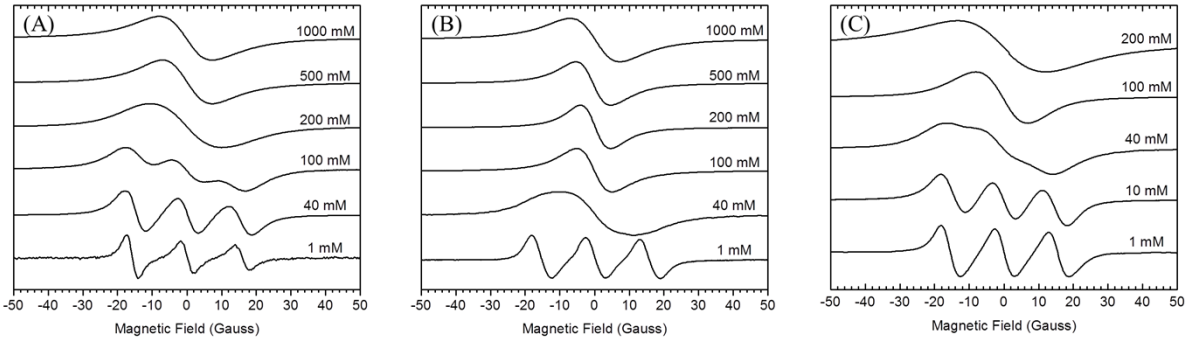

Figure S1: EPR spectra of TEMPOL in a) DMSO b) Acetone and c) Toluene as a function of the radical concentration. EPR spectra are recorded at 180 GHz MW frequency and 25°C temperature. The magnetic field axis is centered with respect to the EPR line (approximately 6.4 T).

The widths of the EPR spectra extracted at G-band (non-degassed samples) are given in Table S1.

Concentration [mM]	DMSO	Acetone	Toluene
1	3.56	3.72	3.70
10			3.63
40	3.63	2.18	3.07
100	3.45	1.03	1.50
200	2.10	0.86	2.52
500	1.46	1.00	
1000	1.54	1.43	

Table S1: Peak-to-Peak line width in [mT] measured at 180 GHz and 25°C

Measurements at low concentrations (< 40 mM) at X-band allowed an estimation of the Heisenberg exchange rate k_e from the change in the linewidth and the hyperfine splitting by the following equations[1]:

$$k_e = 1.52 \cdot 10^7 \frac{g \quad \Delta B}{2(1-\varphi) \; c} \quad \text{(from line broadening)}$$

$$k_e = 1.76 \cdot 10^7 \frac{g \; \Delta B \; \sqrt{A_{iso} \cdot \delta A_{iso}}}{2c\sqrt{\varphi} \qquad c} \quad \text{(from change in hyperfine splitting)}$$

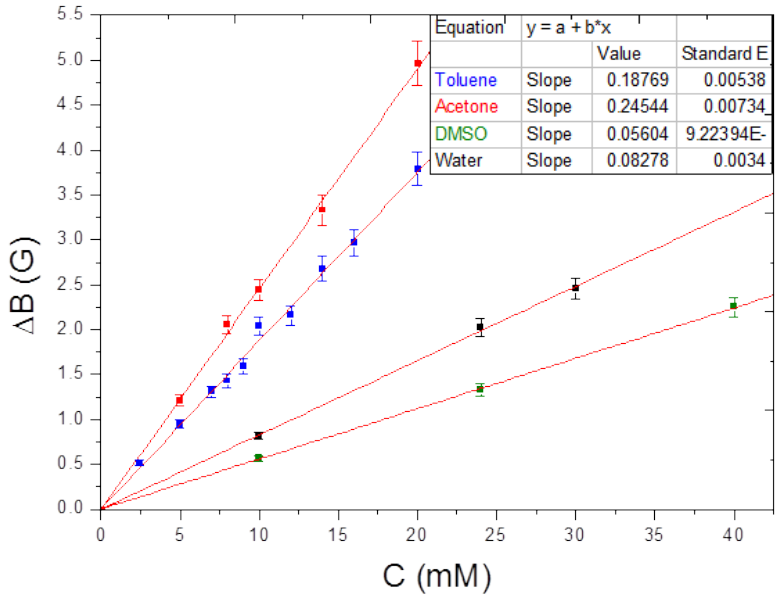

Figure S2: Calculation of Heisenberg exchange rate from the linewidth of single hyperfine line as a function of radical concentration

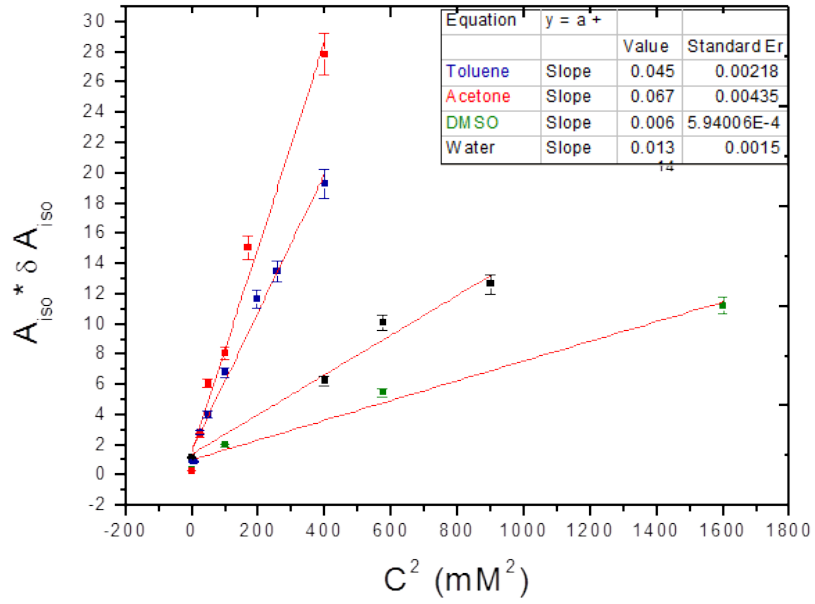

Figure S3: Calculation of the Heisenberg exchange rate from the change of the hyperfine splitting δA_{iso} as a function of the radical concentration

The Heisenberg exchange rates determined from Figures S2 and S3 are given in Table S2. They compare well with rates determined by pulsed ELDOR at X-band frequencies for water and toluene[2].

Solvent	k_e from line broadening [10^{-9} M^{-1} s^{-1}]	k_e from hyperfine coupling [10^{-9} M^{-1} s^{-1}]
DMSO	2.6	1.9
Acetone	11.6	7.2
Toluene	8.7	6.0
Water	3.7	2.4

Table S2: Heisenberg exchange rates k_e determined from X-band EPR spectra as a function of radical concentration

Same rates could be extracted from G-band cw-EPR spectra.

2) Rotational correlation times determined from X-band and G-band cw-EPR spectra

Simulations of the EPR spectra at X-band and G-band by EasySpin[3] for low spin concentrations allowed estimation of the rotational correlation time τ_R of the radicals in the different solvents at room temperature.

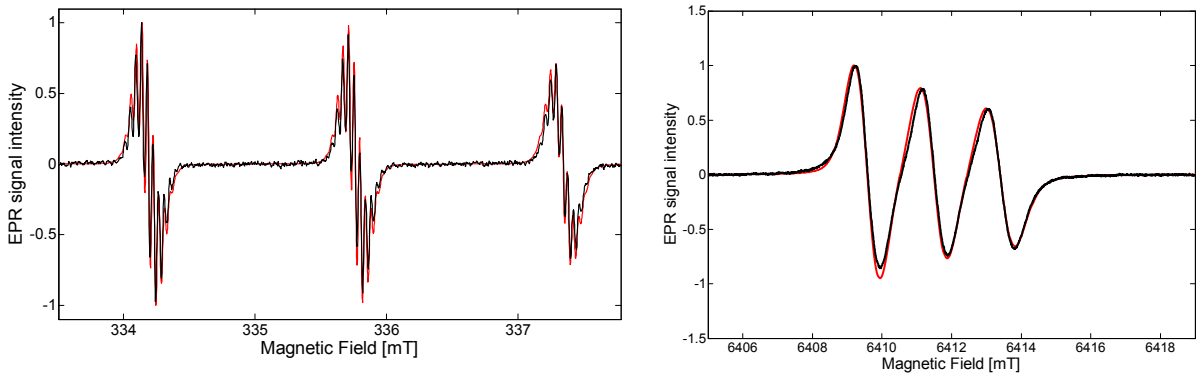

Figure S4: X-band (left, 100 μM) and G-band (right, 5 mM) cw-EPR spectra of TEMPOL in DMSO at RT (black) and fast motion fits with EasySpin (red).

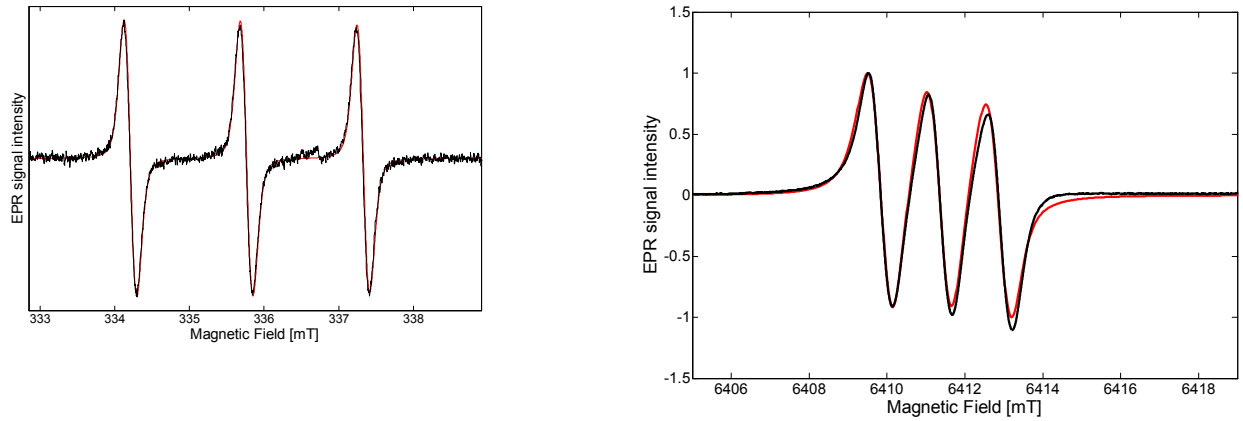

Figure S5: X-band (left, 100 μM) and G-band (right, 5 mM) cw-EPR spectra of TEMPOL in Acetone at RT (black) and fast motion fits with EasySpin (red).

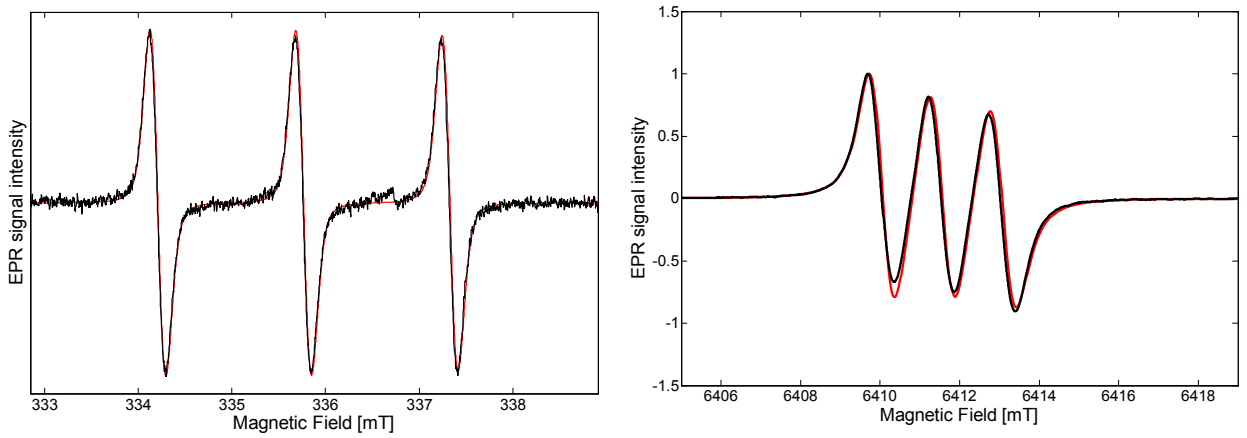

Figure S6: X-band (left, 100 μM) and G-band (right, 2.5 mM) cw-EPR spectra of TEMPOL in Toluene at RT (black) and fast motion fits with EasySpin (red).

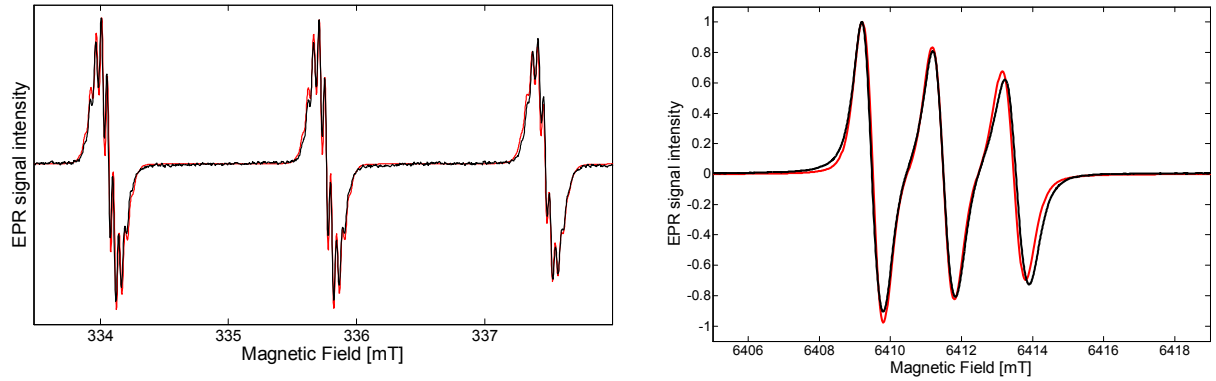

Figure S7: X-band (left, 100 μM) and G-band (right, 10 mM) cw-EPR spectra of TEMPOL in water at RT (black) and fast motion fits with EasySpin (red).

The rotational correlation times determined from the fast motion fits with EasySpin of the X-band and G-band cw-EPR spectra are given in Table S3. Samples for X-band measurements were measured with a radical concentration of 100 μM and degassed before measurements, whereas G-band measurements were performed at higher concentrations 2.5-10 mM without degassing. For the simulations of the G-band spectra a small (<10%) dispersive component had to be taken into account.

Solvent	τ_R [ps] from G-band spectra	τ_R [ps] from X-band spectra
DMSO	34	27
Acetone	10	10
Toluene	12	15
Water	22	19

Table S3: Rotational correlation times τ_R determined from fast motion fits of X-band and G-band cw-EPR spectra

3) Temperature calibration of samples under DNP conditions

In order to assign the sample temperature under MW irradiation DNP conditions we performed a temperature calibration based on the temperature dependent relative shift ($\Delta\delta$) between the OH and the CH_2 peaks of ethylene glycol[4], which was added 10% to DMSO and acetone (peaks shown as inset in

Figure B). In part A of the Figures the change of $\Delta\delta$ upon heating of the sample by a gas flow is compared for a classical Bruker BBI liquid NMR probe and the tiny DNP samples in our home-build double resonance DNP probe. In part B of the Figures these differential chemical shift $\Delta\delta$ in the DNP probe is observed under MW irradiation conditions, allowing calibrating the temperature of the DNP samples for a given MW power. Part C of the Figures shows the chemical shift of the two solvents (DMSO and Acetone) under MW irradiation. Temperature calibrations for both solvents DMSO and Acetone are done for 50 µm ID capillaries.

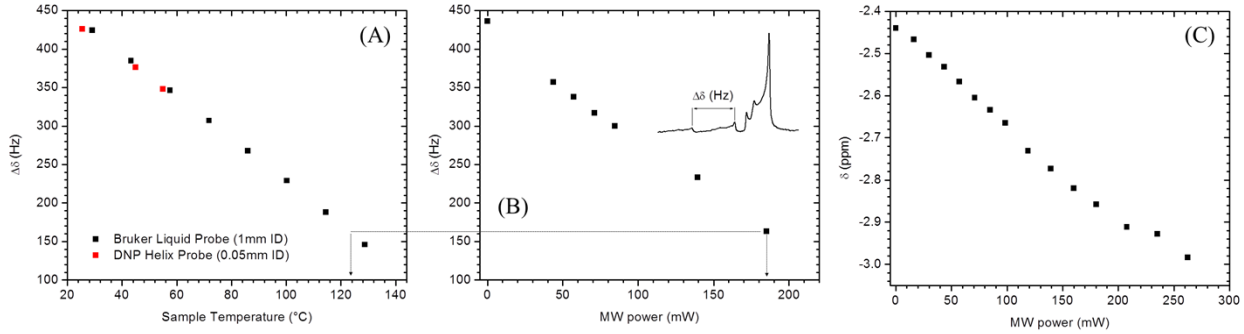

Figure S8: Temperature calibration curves for DMSO solvent. A) Differential chemical shift of 10% glycerol in DMSO as a function of temperature. Black: NMR probe, Red: DNP probe. B) Differential chemical shift of 10% glycerol peaks as a function of applied MW power. Insert: NMR spectra where the glycerol peaks used for temperature calibration are indicated by arrows. C) Chemical shift of the DMSO proton signal by applied MW power.

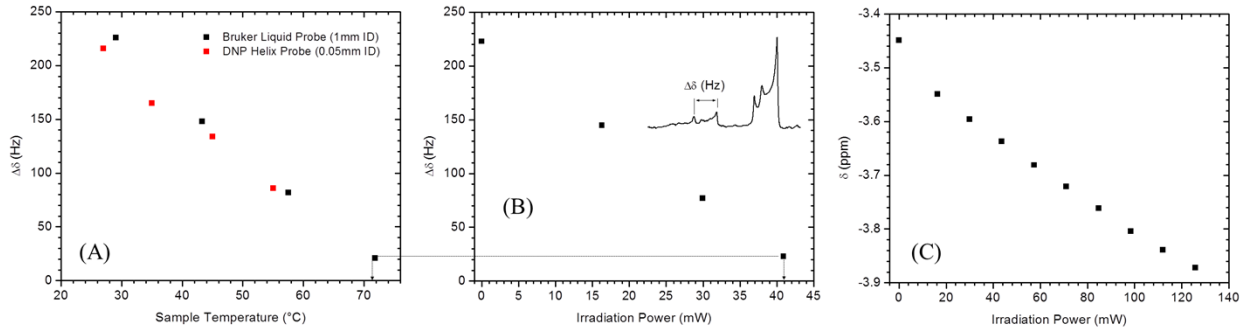

Figure S9: Temperature calibration curves for Acetone solvent. A) Differential chemical shift of 10% glycerol in Acetone as a function of temperature. Black: NMR probe, Red: DNP probe. B) Differential chemical shift of 10% glycerol peaks as a function of applied MW power. Insert: NMR spectra where the glycerol peaks used for temperature calibration are indicated by arrows. C) Chemical shift of the Acetone proton signal by applied MW power.

4) Leakage factor determination at different temperatures and radical concentrations

Leakage factors have been determined for all used radical concentrations at several temperatures for all solvents by measuring the proton relaxation rate with and without radicals. Leakage factors at RT and some selected elevated temperatures together with T_1 relaxation times of the pure solvents are given in Table S4.

Concentrations	200 mM	100 mM	40 mM	20 mM	5 mM	pure solvent T_1 [s]
DMSO (25 °C)	0.99	0.98	0.95	0.89	0.69	2.7
DMSO (135 °C)	0.99	0.97	0.93	0.86	0.64	10.3
Acetone (25 °C)	0.98	0.93	0.85	0.62	0.26	2.8
Acetone (55 °C)	0.98	0.92	0.86	0.61	0.25	3.6
Toluene CH_3 / ring (25 °C)	0.98 / 0.99	0.96 / 0.98	0.91 / 0.94	0.85 / 0.89	0.58 / 0.67	4.4 / 5.4
Toluene CH_3 / ring (65 °C)	0.98 / 0.99	0.95 / 0.97	0.89 / 0.93	0.81 / 0.87	0.51 / 0.62	5.6 / 7.7
Water (25 °C)	0.99	0.98	0.95	0.90	0.66	3.0
Water (95 °C)	0.99	0.98	0.94	0.89	0.64	10.0

Table S4: Leakage factors for different radical concentrations and temperatures for all solvents used. The last row gives the T_1 relaxation times of the pure solvents.

5) Saturation parameter as a function of MW power

The saturation parameter as a function of MW power has been determined by observing the suppression of the paramagnetic shift of the proton NMR line as a function of applied MW power for 1M radical concentrations. To obtain saturation curves the chemical shift change induced by MW heating has to be corrected, which was done by performing reference experiments on samples without radicals[4]. As can be seen high saturation values have been obtained for all solvents at a MW power of > 100 mW. Sample heating as well as saturation behavior depends on the capillary size as shown in the following Figures. Non asymptotic behavior of the enhancement and chemical shift curves for some larger size capillary might be caused by convection within the capillary[5] and/or inhomogeneous MW field distribution over the sample size.

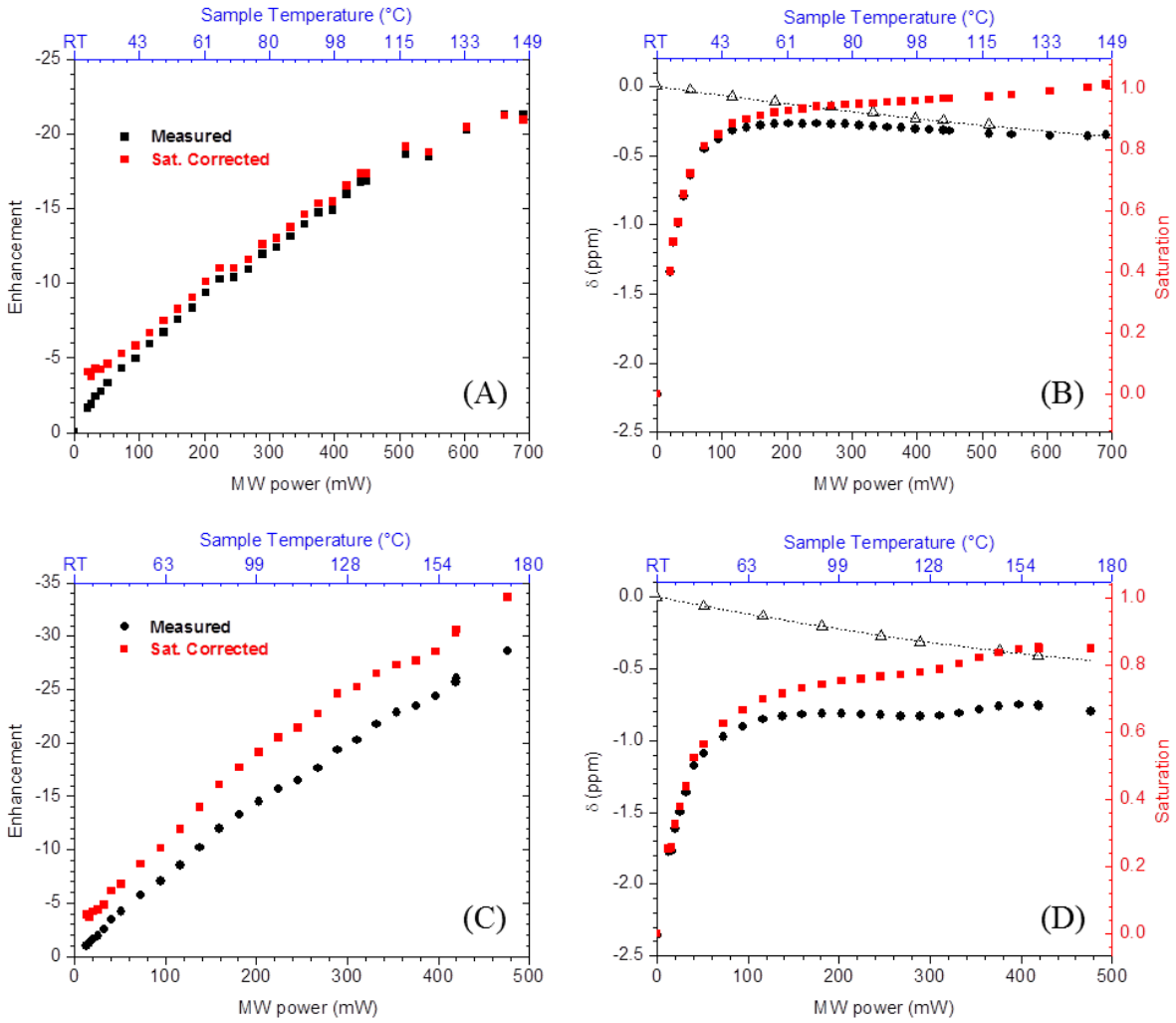

Figure S10: DNP enhancement (A/C) and chemical shift (B/D) as a function of MW power for DMSO solvent. (A,B): ID capillary size of 20 µm. (C,D): ID capillary size of 30 µm. (A/C): experimentally measured DNP enhancement factor by integration over the whole NMR line (black circles), after correction with the saturation factor extracted from diagram B and D respectively (red squares). (B/D) measured chemical shift as a function of applied MW power for 1M TEMPOL (black circles), measured chemical shifts for pure solvent (open triangles) and corrected paramagnetic shifts with respective saturation values given by the scale at the right side (red squares).

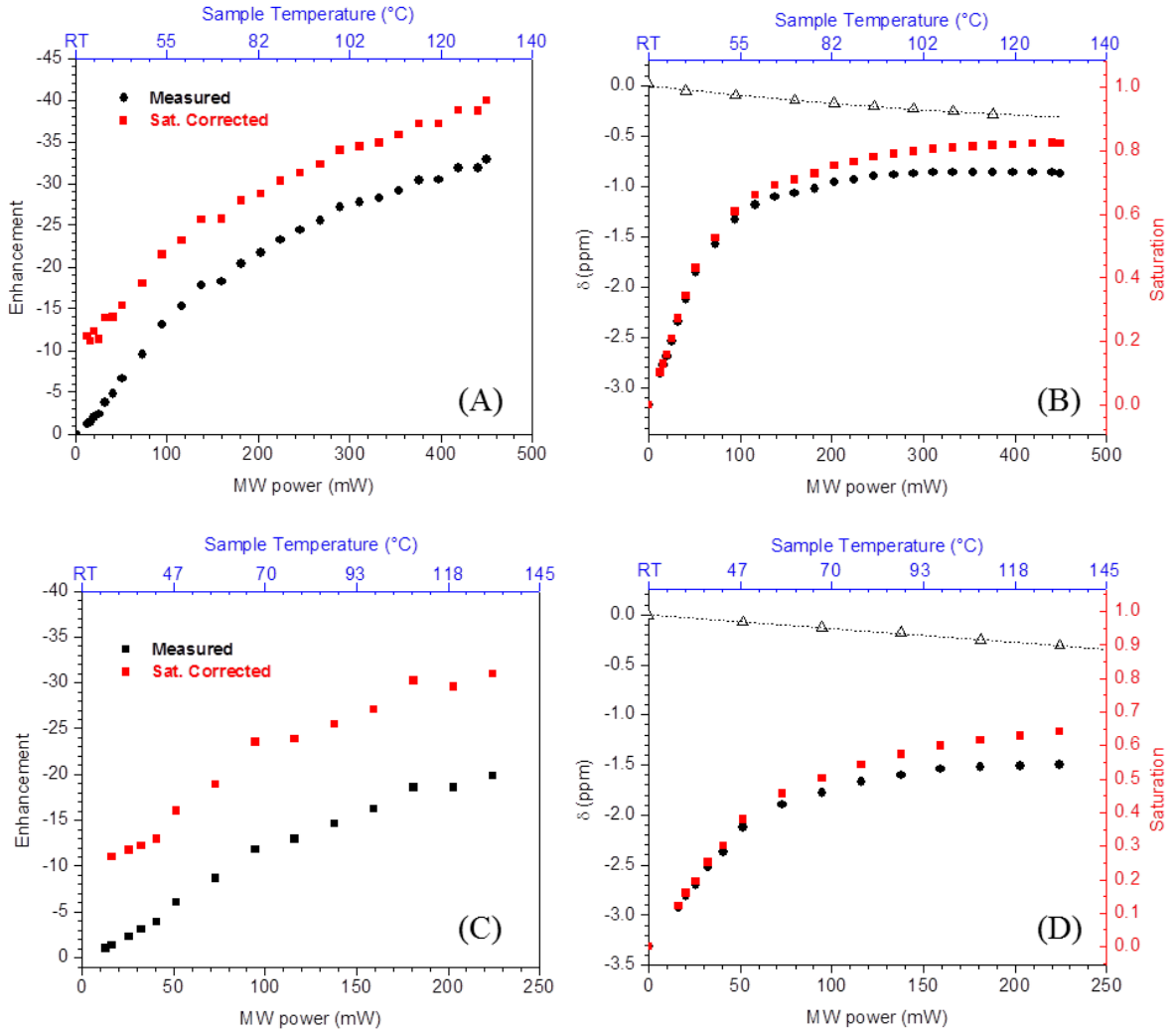

Figure S11: DNP enhancement (A/C) and chemical shift (B/D) as a function of MW power for Acetone as solvent. (A,B): ID capillary size of 20 µm. (C,D): ID capillary size of 30 µm. (A/C): experimentally measured DNP enhancement factor by integration over the whole NMR line (black circles), after correction with the saturation factor extracted from diagram B and D respectively (red squares). (B/D) measured chemical shift as a function of applied MW power for 1M TEMPOL (black circles), measured chemical shifts for pure solvent (open triangles) and corrected paramagnetic shifts with respective saturation values given by the scale at the right side (red squares).

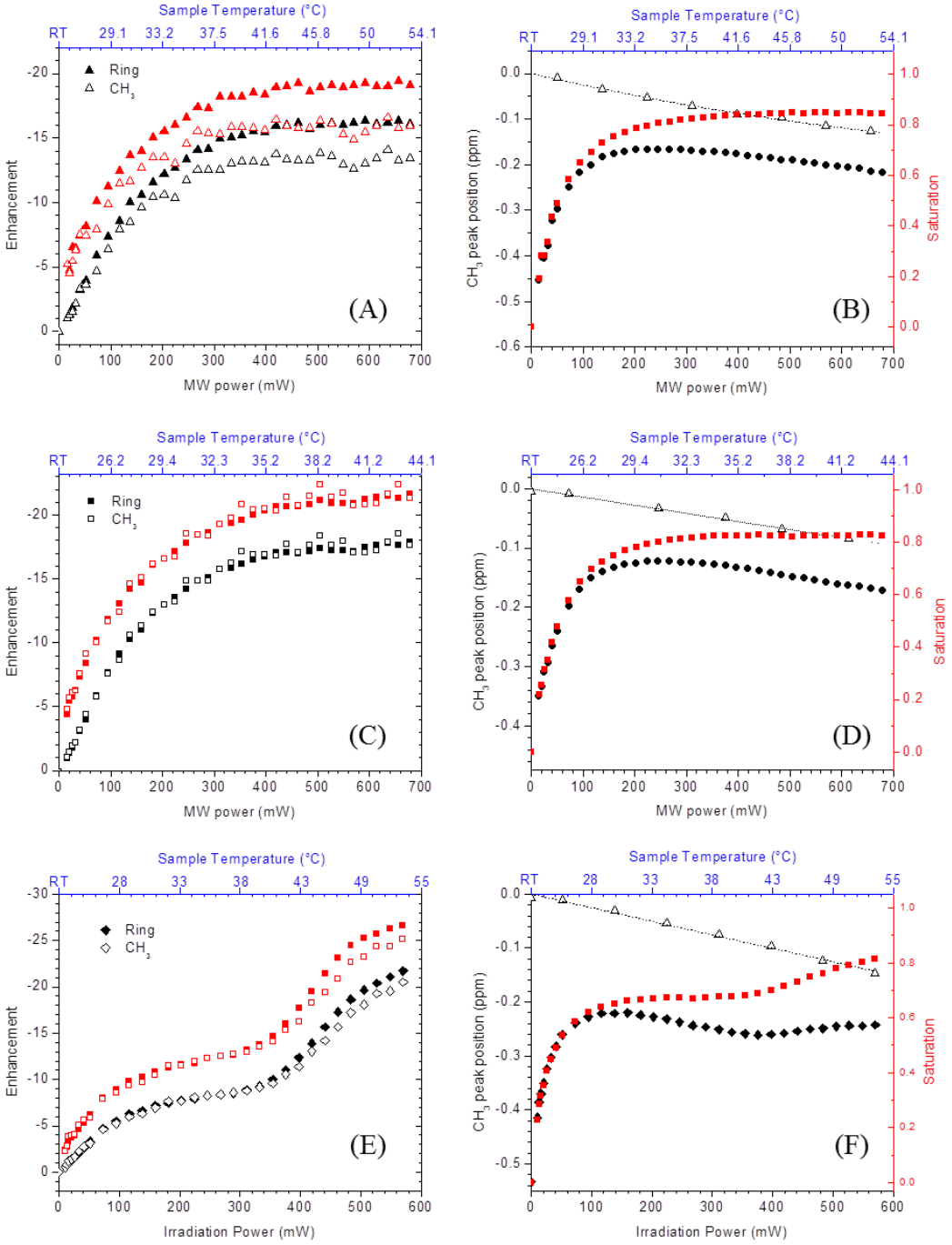

Figure S12: DNP enhancement (A/C/E) and chemical shift (B/D/F) as a function of MW power for Toluene as solvent. (A,B): ID capillary size of 30 µm. (C,D): ID capillary size of 50 µm and (E/F): ID capillary size of 100 µm. (A/C/E): experimentally measured DNP enhancement factor by integration over the whole NMR line (black circles), after correction with the saturation factor extracted from diagram B, D and F respectively (red squares). (B/D/F) measured chemical shift as a function of applied MW power for 1M TEMPOL (black circles), measured chemical shifts for pure solvent (open triangles) and corrected paramagnetic shifts with respective saturation values given by the scale at the right side (red squares).

6) NMRD measurements

Solvent ^{1}H NMRD profiles for solutions of ^{14}N-TEMPOL in DMSO (Figure S13) and toluene (Figure S14) are shown at different temperatures ranging from 25 to 80 °C. Best fit profiles are also shown as lines (outer-sphere model A in blue, outer-sphere and inner-sphere model B in red**,** model C with inner-sphere correlation time adjusted to fit NMRD and DNP data in green). Models B and C (red and green curves) are in a sizably better agreement with the experimental data than model A (blue curves) for DMSO, although only in slightly better agreement for toluene.

The parameters obtained from the fits of the NMRD measurements are given in Table S5 (DMSO), S6 (acetone) and S7 (toluene).

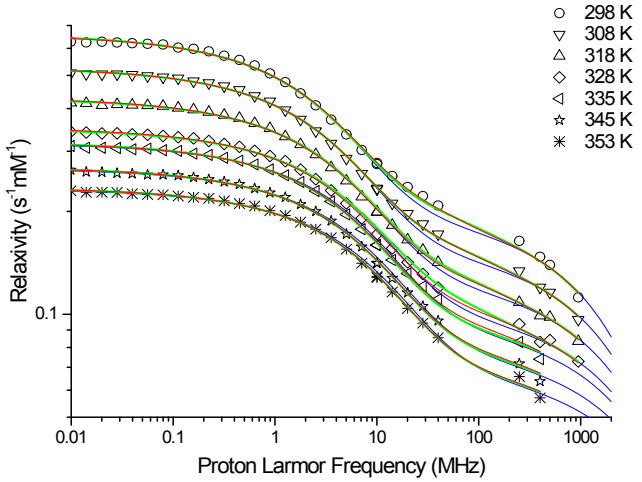

Figure S13: NMRD profiles for DMSO as solvent at different temperatures together with fits with Model A (blue), B (red) and C (green). See text for more details on the different models.

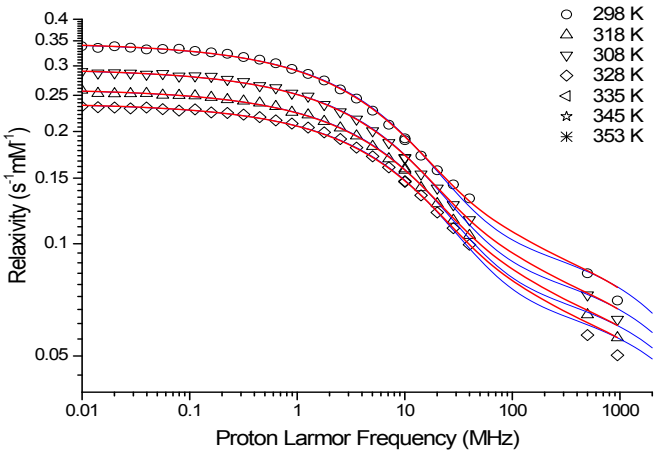

Figure S14: NMRD profiles for toluene as solvent at different temperatures together with fits with Model A (blue) and B (red). See text for more explanations.

	T (K)	298	308	318	328	335	345	353
Model A	d (Å)	3.64 ± 0.01						
	D (10^{-9} m^2/s)	1.15 ± 0.01	1.44 ± 0.01	1.77 ± 0.01	2.17 ± 0.01	2.40 ± 0.01	2.84 ± 0.02	3.26 ± 0.02
	$\tau_D (=d^2/D)$ (ps)	115	92	75	61	55	47	41
Model B	d (Å)	3.82 ± 0.03						
	D (10^{-9} m^2/s)	1.13 ± 0.01	1.41 ± 0.01	1.74 ± 0.01	2.13 ± 0.01	2.35 ± 0.01	2.79 ± 0.02	3.20 ± 0.02
	$\Sigma_i n_i/r_i^6$ (Å^{-6})	0.0046 ± 0.0012						
	τ_c (ps)	1.57 ± 0.44	1.26 ± 0.36	1.03 ± 0.29	0.85 ± 0.24	0.75 ± 0.21	0.63 ± 0.18	0.55 ± 0.16
Model C	d (Å)	3.80 ± 0.02						
	D (10^{-9} m^2/s)	1.14 ± 0.01	1.42 ± 0.01	1.73 ± 0.01	2.11 ± 0.02	2.32 ± 0.02	2.73 ± 0.03	3.13 ± 0.04
	$\Sigma_i n_i/r_i^6$ (Å^{-6})	0.0023 ± 0.0010						
	τ_c (ps)	3.71 ± 0.31	2.45 ± 0.30	1.55 ± 0.29	0.97 ± 0.30	0.75 ± 0.30	0.43 ± 0.30	0.29 ± 0.29

Table S5: Fit parameters of the NMRD profiles for the solvent DMSO. Model A represent fits with only outer-sphere diffusional motion with correlation time τ_D , Model B with additional inner-sphere complex motion with an additional correlation time τ_c with a temperature dependence described by Eq.7 in the paper, Model C with τ_c fixed to sub-picoseconds only for the three higher temperatures.

T (K)	298	308	318	328
d (Å)	3.34 ± 0.02			
D (10^{-9} m^2/s)	4.94 ± 0.03	5.61 ± 0.04	6.12 ± 0.04	6.58 ± 0.04
$\tau_D(=d^2/D)$ (ps)	23	20	18	17

Table S6: Fit parameters of the NMRD profiles for the solvent acetone, where only outer-sphere relaxation has been taken into account (Model A).

	T (K)	298	308	318	328	335	345	353
Model A	d (Å)	3.25 ± 0.01						
	D (10^{-9} m^2/s)	2.46 ± 0.01	2.89 ± 0.01	3.27 ± 0.01	3.57 ± 0.01	3.79 ± 0.01	4.16 ± 0.02	4.37 ± 0.02
	$\tau_D(=d^2/D)$ (ps)	43	37	32	30	28	25	24
Model B	d (Å)	3.45 ± 0.04						
	D (10^{-9} m^2/s)	2.42 ± 0.01	2.85 ± 0.01	3.23 ± 0.01	3.52 ± 0.02	3.74 ± 0.02	4.10 ± 0.02	4.30 ± 0.02
	$\Sigma_i n_i/r_i^6$ ($Å^{-6}$)	0.0028 ± 0.0005						
	τ_c (ps)	1.54 ± 0.30	1.39 ± 0.27	1.25 ± 0.25	1.14 ± 0.22	1.07 ± 0.21	0.98 ± 0.19	0.92 ± 0.18

Table S7: Fit parameters of the NMRD profiles for the solvent toluene. Model A represent fits with only outer-sphere diffusional motion with correlation time τ_D , Model B with additional inner-sphere complex motion with an additional correlation time τ_c with a temperature dependence described by Eq.7 in the paper.

1. Yu. N. Molin, K. M Salikhov, K. I. Zamaraev, Spin Exchange, Springer-Verlag Berlin, Heidelberg, New York, 1980.
2. N. Enkin, G. Liu, I. Tkach, M. Bennati, *Phys. Chem. Chem. Phys.,* 2014, **16**, 8795-8800.
3. S. Stoll, A. Schweiger, *J. Mag. Reson.,* 2006, **178**, 42-55.
4. P. Neugebauer, J. G. Krummenacker, V. P. Denysenkov, G. Parigi, C. Luchinat and T. F. Prisner, *Phys. Chem. Chem. Phys.*, 2013, **15**, 6049-6056 .
5. P. J. M. van Bentum, G. H. A. van der Heijden, J. A. Villanueva-Garibay, A. P. M. Kentgens, *Phys. Chem. Chem. Phys.,* 2011, 13, 17831-17840.